STRETCHABLE, SOFT, AND WIRELESS BIOMEDICAL ELECTRONICS

BY

HA UK CHUNG

THESIS

Submitted in partial fulfillment of the requirements
for the degree of Master of Science in Electrical and Computer Engineering
in the Graduate College of the
University of Illinois at Urbana-Champaign, 2016

Urbana, Illinois

Advisor:

Professor John A. Rogers

ABSTRACT

Electrophysiology that records various bio-signals from living organisms has broad impacts on clinical diagnosis and study. Having a recording system, effectively small and compatible with wireless communication, not only leads to the new environment in which health monitoring can commonly take place outside the hospital with portable recording devices, but also contributes to development in neuroscience by enabling studies on neural activity with the help of an implantable neural interface. This thesis presents a soft, stretchable, and wireless biomedical electronics system for both skin-mountable and implantable applications. The wireless capability associated with Bluetooth Low Energy (BLE) allows continuous monitoring in portable devices in user-friendly environments. Furthermore, the mechanical superiority of the flexible and stretchable platform enables this type of system to be implanted in a living rat to record and stimulate a pelvic nerve.

ACKNOWLEDGMENTS

I would like to thank my advisor, Professor John A. Rogers, for providing great support throughout my academic research career. He has been guiding me with great insight and passion. I would like to thank academic mentors including Professor Sung Hun Jin, Dr. Sung Il Park, and Dr. Kyung-In Jang for being great mentors in various research projects that I have been involved with. In addition, I would like to thank all the collaborators including Professor R. Gereau and his group members at Washington University in St. Louis, Professor S. Lewis and Dr. Yee Hsee Hsieh at Case Western Reserve University, Dr. Gunchul Shin and Dr. Jangyeol Yoon at University of Illinois at Urbana-Champaign. Also, I would like to thank Jong Yoon Lee for assisting me. Finally, I would like to thank my family for everything.

This work was supported by GSK Innovation Challenge.

TABLE OF CONTENTS

CHAPTER 1: Introduction

Since 1929, recording physiological signals on the skin has attracted much research interest [1]. Recently, an electronic system, so-called 'epidermal electronics', which can be attached on skin and perform continuous physiological monitoring with multiple other functionalities, has been reported in 2011 [2]. This new electronic system led to improvements in not only skin-mountable electronic systems with enhanced functionality, but also implantable electronic systems with various target applications such as implantable optogenetics [3, 4]. The system described in this thesis has also been originated and motivated by the epidermal electronics.

In developing both skin-mountable and implantable wireless devices, the main design consideration of the biomedical recording system is the electrical functionality. The main functionality in both devices is to measure electrophysiological signals of living organisms. While the skin-mountable device aims to monitor bio-signals on the skin of a human being, the implantable device is specifically designed to control the bladder activity of a rat by recording and stimulating the pelvic nerve. The wireless communication capability significantly improves the portability of the skin-mountable device, while the nature of the implantable device strictly requires wireless communication. Therefore, the wireless mode is a crucial design aspect. In addition, the implantable system requires a secondary source of power supply as the limited space for implantation in a rat significantly restricts the capacity of the battery available. As a secondary

source of power, the wireless charging scheme based on inductive coupling is developed. In this way, a small rechargeable battery can be used to power up the implantable device with the wireless charging station.

Another important design aspect is the mechanical properties, which include low effective modulus, bending stiffness, and conformal contact. In addition, all functional blocks are connected with serpentine metal interconnects, which makes the system stretchable and its shape recoverable without mechanical deformation. The overall device is passivated by silicon based polymer. The soft and stretchable platform improves the suitability in both skin-mountable applications with conformal contact and implantable applications by making the system easier to implant into spots which are difficult for the rigid system to access.

CHAPTER 2: A Skin-mountable Wireless Recording System

This chapter introduces a type of wireless device that can be attached on the skin and record electrophysiological signals and acceleration from hand movement.

2.1. System Overview

The system in high-level overview consists of wireless recording system and base station with custom graphical user interface (GUI) developed on Android environment (Figure 2.1). The wireless recording system consists of three main components: recording circuit, digital accelerometer, and Bluetooth system-on-a-chip (SoC). The steps of recording the signal are illustrated in Figure 2.2.

The raw signal from the differential input measured by two surface electrodes is amplified through an instrumentation amplifier (INA333, Texas Instruments; common-mode rejection ratio (CMRR) of 100 dB). The instrumentation amplifier is chosen because of its high CMRR and flexible gain selection. In addition, the bandwidth of the instrumentation amplifier is 3.5 kHz at the gain of 100, which is wide enough for this application. As a pre-amplification stage, the gain of the instrumentation amplifier is set to 100. The final gain of 10,000 is achieved at the non-inverting configuration of operation amplifier (OPA333, Texas Instruments) with the gain of 100.

The Sallen-Key filter topology is used in filter stage based on its high input impedance, tunable gain, small output impedance, and high Q factor. The passband and final gain should be determined based on measurement specifications. The sEMG signal has a passband of 10-500 Hz and a gain of 10,000 [5].

A digital accelerometer (ADXL345, Analog Devices) is a part of the recording system that measures the vibration of a forearm. It has been reported that the acceleration signal and sEMG signal can be used in tremor diagnosis for clinical studies [6, 7]. While the current prototype is only to record raw signals, future applications will involve the tremor diagnosis. The digital accelerometer consists of a 3-axis accelerometer sensor with signal processing unit including analog-to-digital converter (ADC) [8]. The communication protocol between microcontroller and the accelerometer used in this application is the serial interface peripheral (SPI). The general SPI mode consists of four logic signals: serial clock (SCK), master output slave input (MOSI), master input slave output (MISO), and slave select (CS). The SCK provides the overall clock signal during the communication and the CS is active low during each clock cycle. The MOSI and MISO signals are meant for exchanging command code and data signals. These can be used alternatively depending on which device acts as master or slave.

The base station is a smartphone with Bluetooth Low Energy (BLE) connectivity. It collects data that is being transmitted from the skin-mountable device and displays the result on the screen. The GUI is developed on Android platform using Android Studio. It consists of raw accelerometer data displayed in numbers, graphical plots of

electrophysiological data and accelerometer data, and data logger with on/off switch, as shown in Figure 2.3.

2.2. System Block

2.2.1. Wireless Communication

Wireless communication is an important aspect of the system that enables the device to transmit recorded data without wires. The design focuses on user-friendly environment with smart devices that are widely available to enhance portability. Other important specifications include reasonable transmission range, data rate, and power consumption. Bluetooth Low Energy (BLE) is a 2.4 GHz protocol with enhanced power management compared to classic Bluetooth at the expense of limited functionality including slower data rate and transmission range. BLE has a reasonable data rate of 1 Mbit/s or below and can transmit over a range of meters [9]. There are other wireless protocols including Wi-Fi and Near Field Communication (NFC). However, Wi-Fi consumes far more power than BLE with current consumption of 200 mA at operating voltage of 3.6 V [10]. In addition, Near Field Communication (NFC) that operates at 13.56 MHz is more power efficient, but the communication range is limited in centimeter range [11]. These properties make BLE a better candidate than other protocols.

A BLE SoC (nRF51822, Nordic Semiconductor) is chosen for wireless communication. It operates at 1.8-3.6 V, which is compatible with the operating voltage of the skin-mountable device of 3 V. The current

consumption is around 10 mA with the radio power at 0 dbm. It consists of microcontroller, radio, internal ADC with 8- to 10-bit conversion, timer, and memory. In addition, it supports SPI protocol for connectivity to peripheral digital devices. The sampling rate of 1 kHz is achievable at the connection interval of 7.5 ms, which satisfies the specification required for sEMG measurement. The transmission range is experimentally tested on the skin in the normal office environment and the result is shown in Table 2.1. Based on the result with current consumption information, the optimum radio power is chosen to be -8 dBm in this application.

The SoC firmware is programmed using Keil-ARM Microcontroller Development Kit μVision 5. The high level overview of firmware controlling nRF51822 SoC is shown in Figure 2.4. The firmware sends one packet consisting of 20 bytes: 14 bytes of electrophysiological data digitized by internal ADC with 8-bit conversion and 6 bytes of 3-axis acceleration data of which each of the x, y, and z-axes takes two bytes. The default SPI setting of the ADXL 345 accelerometer is most significant bit (MSB) first, clock polarity (CPOL) = 1, and clock phase (CPHA) = 1. The accelerometer data of ADXL345 is collected with ±16g at 10-bit resolution. Timers control various things including sampling rate of ADC, advertising interval, connection interval, and interrupt handler. The sampling rate is chosen to be at 1 kHz and transmission data rate is 21333 bps.

2.2.2. Recording Circuit

The recording circuit is shown in Figure 2.5. As a pre-amplifier, an instrumentation amplifier (INA333) is used. The gain is set as 100 with

external resistor, R_G, with 1 kΩ connected. Differential inputs are connected to surface electrodes through 2.8 kΩ resistors. The reference pin of INA333 is connected by the 1.5 V output of DC offset stage. The DC offset stage is required to capture the negative component of the electrophysiological signal. Since the instrumentation amplifier is fed by a single power supply with 3 V, the DC offset of 1.5 V should be kept as the reference level to capture the full waveform. This is done by having the operational amplifier (OPA333) in unity-gain voltage follower configuration, fed by voltage-divided input from 3 V to 1.5 V. The filtering stage is composed of a low-pass filter and high-pass filter. The filter topology used here is a Sallen-Key topology that is a second-order active filter. It is a voltage-controlled voltage source (VCVS) filter topology with properties of high input impedance, small output impedance, and 2-pole responses with high Q factor. These properties are the factors considered in choosing filters in the recording circuit.

The general expression for transfer function of the Sallen-Key filter can be calculated with the Figure 2.6. The input voltages of the operational amplifier, V_+ and V_-, are matched ($V_+ = V_-$). In addition, the operational amplifier is in negative-feedback configuration, resulting in $V_+ = V_- = V_{out}$.

$$\boldsymbol{V_+ = V_- = Vout} \tag{2.1}$$

Then, a Kirchhoff's current law (KCL) can be applied at the node V_X.

$$\frac{\boldsymbol{V_{in} - V_x}}{\boldsymbol{Z_1}} + \frac{\boldsymbol{V_+ - V_x}}{\boldsymbol{Z_2}} + \frac{\boldsymbol{V_{out} - V_x}}{\boldsymbol{Z_3}} = \boldsymbol{0} \tag{2.2}$$

Also, another KCL equation can be obtained at the node V_+.

$$\frac{\boldsymbol{V_+ - V_x}}{\boldsymbol{Z_2}} + \frac{\boldsymbol{V_+}}{\boldsymbol{Z_4}} = \boldsymbol{0} \tag{2.3}$$

After applying Equation (2.1) to Equation (2.3), Equation (2.3) can be

rearranged to Equation (2.4).

$$\boldsymbol{V_x = V_{out}\left(\frac{Z_2}{Z_4} + 1\right)} \tag{2.4}$$

Finally, applying Equation (2.1) and (2.4) to Equation (2.2) and rearranging gives the transfer function shown in Equation (2.5).

$$\boldsymbol{\frac{V_{out}}{V_{in}} = \frac{Z_3 Z_4}{Z_1 Z_2 + Z_3(Z_1 + Z_2) + Z_3 Z_4}} \tag{2.5}$$

Using the transfer function obtained in Equation (2.5), the transfer function of the low-pass filter and high-pass filter can be obtained. In case of a low-pass filter, the impedances can be defined as $Z_1 = R_1,\ Z_2 = R_2,\ Z_3 = \frac{1}{sC_1}$, $Z_4 = \frac{1}{sC_2}$. Applying these values to the original transfer function, the transfer function of a low-pass filter is found in Equation (2.6).

$$\boldsymbol{\mathbf{H(s)} = \frac{{\omega_0}^2}{s^2 + 2\alpha s + {\omega_0}^2}} \tag{2.6}$$

$$\boldsymbol{\omega_0 = \frac{1}{\sqrt{R_1 R_2 C_1 C_2}}} \tag{2.7}$$

$$\boldsymbol{\alpha = \frac{1}{2C_1}\left(\frac{R_1 + R_2}{R_1 R_2}\right)} \tag{2.8}$$

In case of a high-pass filter, the impedances can be defined as $Z_1 = \frac{1}{sC_1}$, $Z_2 = \frac{1}{sC_2},\ Z_3 = R_1,\ Z_4 = R_2$. Then, the transfer function of a high-pass filter is found in Equation (2.9).

$$\boldsymbol{\mathbf{H(s)} = \frac{{\omega_0}^2}{s^2 + 2\alpha s + {\omega_0}^2}} \tag{2.9}$$

$$\boldsymbol{\omega_0 = \frac{1}{\sqrt{R_1 R_2 C_1 C_2}}} \tag{2.10}$$

$$\boldsymbol{\alpha = \left(\frac{C_1 + C_2}{2R_2 C_1 C_2}\right)} \tag{2.11}$$

Based on these parameters, the desired passband of the recording circuit from 10 Hz to 500 Hz is achieved with the component values as shown in

Figure 2.5. The frequency response of the overall recording circuit is shown in Figure 2.7. It shows that the overall gain within the passband is about 80 dB, which is 10,000 as desired. The cutoff frequencies of the low-pass filter and high-pass filter are at 10 and 500 Hz, respectively, at the gain of approximately -3 dB.

2.2.3. Power Consumption

Power consumption is an important factor in system design. Although BLE consumes less power than Wi-Fi and classic BLE, it still consumes significant power. Therefore, careful power management is required.

The sources of power consumption are the nRF51822 SoC, instrumentation amplifier, operational amplifiers (OP-AMP) in filtering and gain stage, and digital accelerometer. Since the skin-mountable system only transmits, the radio power consumption with TX event is only considered in power management. The overall system operates at 3 V and current consumption of each component is described in the Table 2.2. In particular, nRF51822 SoC current consumption is divided into CPU, radio, SPI, and ADC. The total current consumption is calculated to be around 10 mA. If three 11 mAh rechargeable coin cells with 9.5 mm diameter x 2.1 mm height are used, the continuous running time is approximately 3 hours. With larger battery, the running time can be improved significantly. As the skin-mountable device does not have a space limitation, the battery size can be chosen based on application requirements.

2.3. Figures

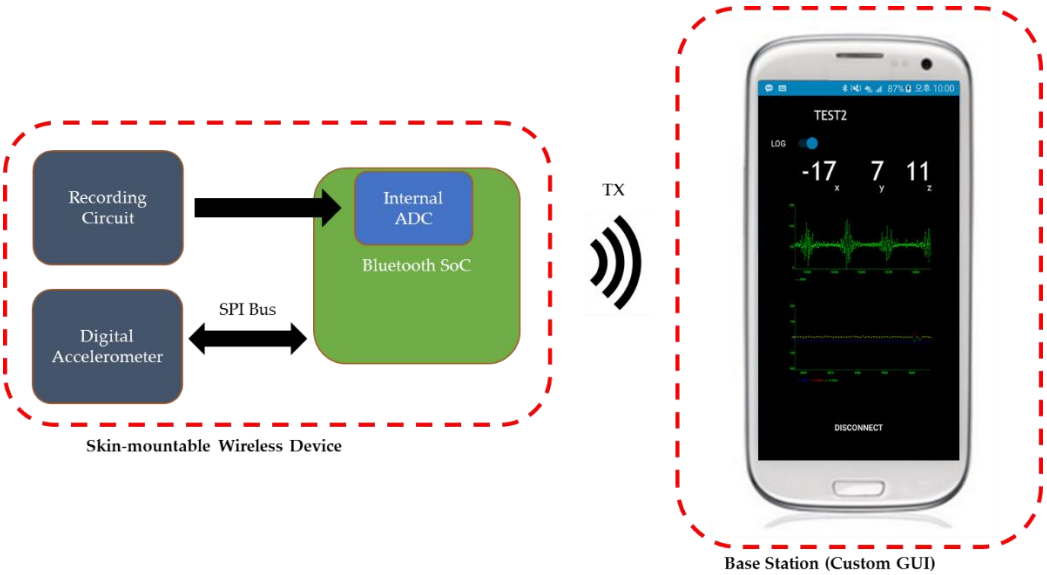

Figure 2.1: High-level system overview of the skin-mountable wireless recording system.

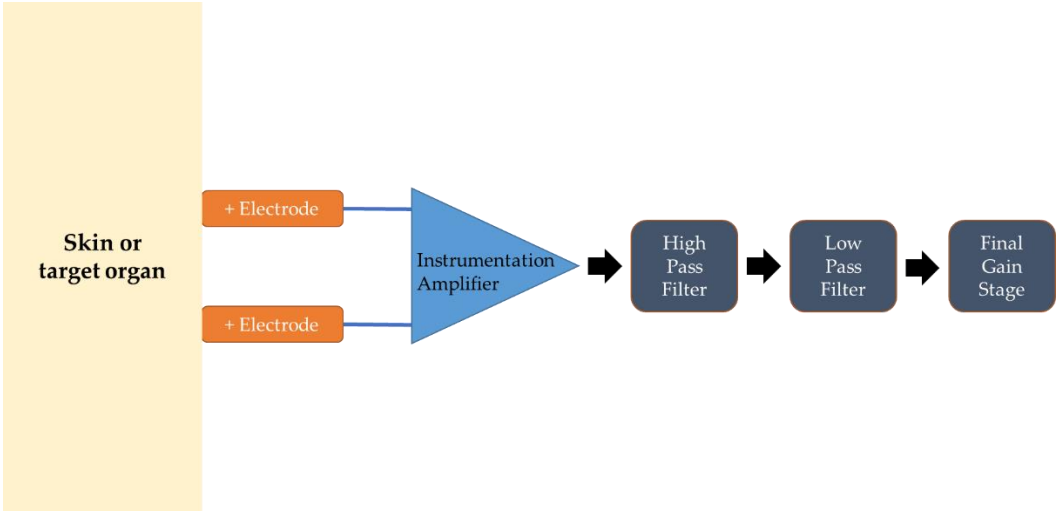

Figure 2.2: Low-level overview of recording stage with amplification and filtering.

Figure 2.3: Android based smartphone GUI developed by Android Studio.

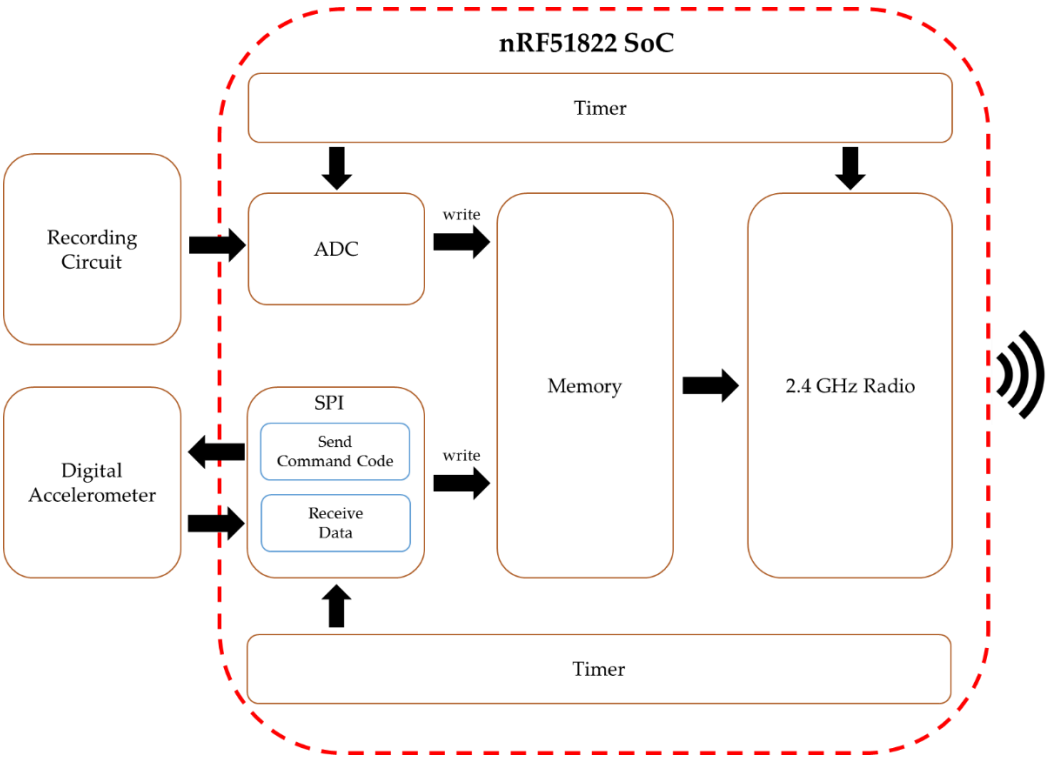

Figure 2.4: High-level overview of firmware of the skin-mountable wireless recording device.

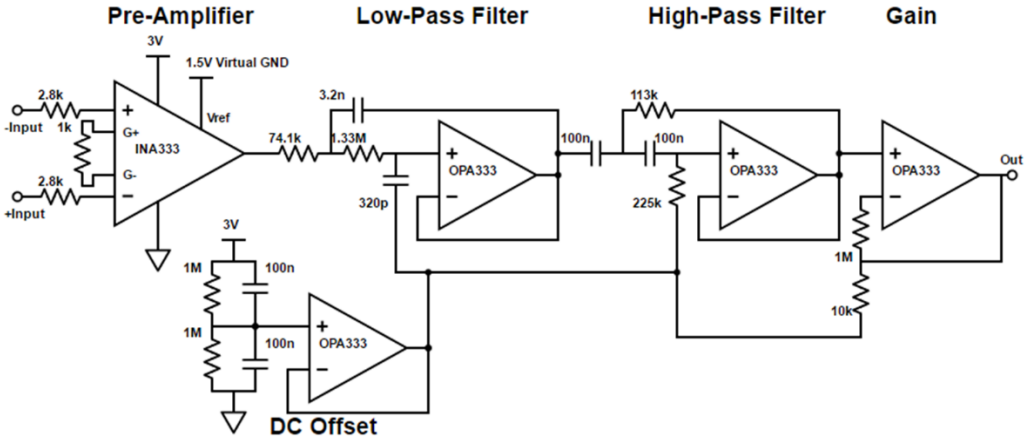

Figure 2.5: The schematic of the recording circuit of skin-mountable device.

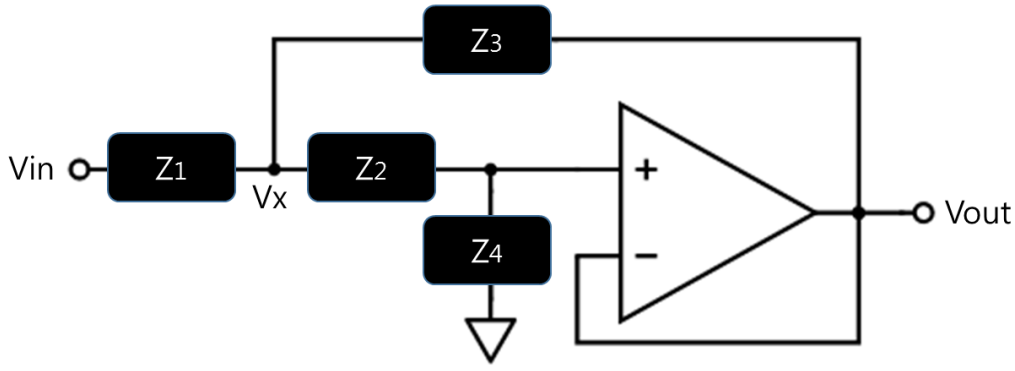

Figure 2.6: A schematic of generic Sallen-Key topology for transfer function calculation.

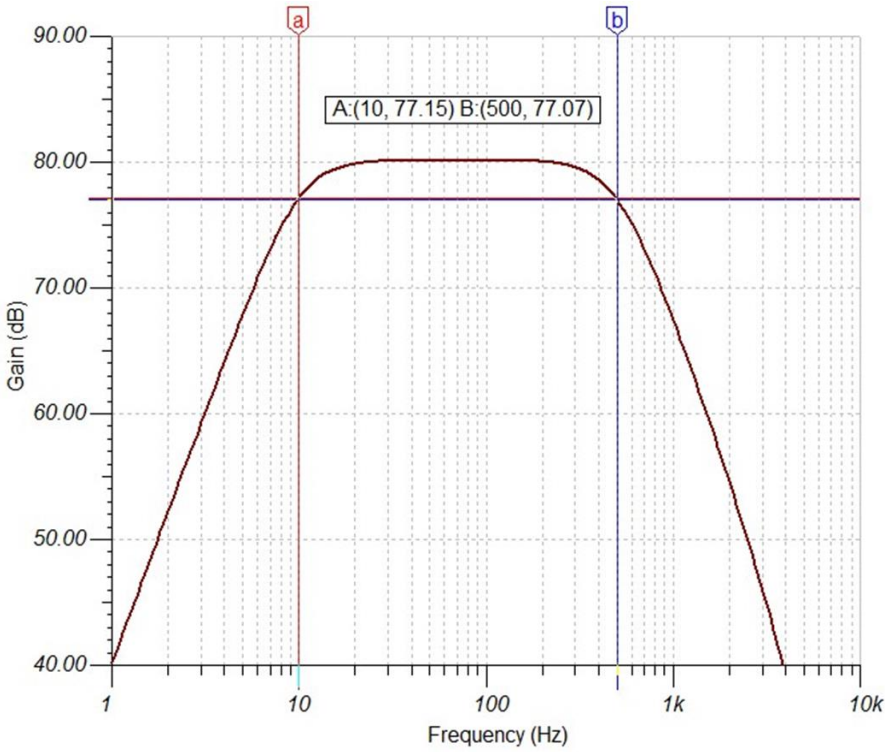

Figure 2.7: The frequency response of the skin-mountable device

2.4. Tables

Table 2.1: Transmission range and current consumption comparison with TX power levels.

TX Power (dBm)	Transmission Range (m)	Current Consumption (mA) [8]
+4	10	16
0	6.5	10.5
-4	3	8
-8	2	7
-12	Less than 1	6.5
-16		6

Table 2.2: The current consumption of the skin-mountable device operating at 3 V.

Components		Current Consumption (mA)
nRF51822 SoC [9]	CPU	2.4
	Radio at -8 dBm	7
	SPI	0.2
	ADC	0.26
Instrumentation Amplifier		0.05
OP AMP x 2		0.034
Digital Accelerometer		0.14
Total Current Consumption		10.084

CHAPTER 3: An Implantable Wireless System

This chapter introduces a type of wireless system that is implantable inside living animals. The target anatomical area is a pelvic nerve to control and record bladder activity of a female rat. The system aims not only to record a neural signaling pattern with a physiological perturbation, but also to stimulate the target nerve to induce the same end-organ function without the perturbation.

3.1. System Requirements

The implantable wireless device is designed particularly for fully-implantable neural recording and stimulation at the pelvic nerve of a female rat. There are various physical and electrical challenges. First, the pelvic nerve is placed in an anatomically difficult region. Thus, the electrode for recording electrophysiological signal needs to be thin, soft, and flexible. Second, the system should be fully implantable, which implies that wireless data communication is essential. In addition, the effective size of the implanted device is at most 3.0 cm x 3.0 cm x 1 cm (W x L x H), considering the space for implantation is quite limited for a typical female rat. This aspect limits the size and capacity of the battery. Thus, it is ideal to have a secondary power source to charge the battery for long operation beyond the battery capacity.

The nerve activity is captured with an external urethral sphincter (EUS) by electromyography (EMG). Acquisition of the nerve signal requires

frequency filtering and signal amplification. As the electrical signals of the nerve are in the microvolt range, the amplifier needs to have a gain of 20,000 or higher. Also, the signal has a passband from 30 Hz to 3 kHz and sampling rate needs to be 1kHz. The effective stimulation condition at the pelvic nerve has been found by performing stimulation at multiple conditions and recording bladder pressure simultaneously using a pressure transducer. The representative figure of the experiment is shown in Figure 3.1. The bladder pressure in all three different stimulation conditions is shown to be reduced greatly. Based on this result, the optimal stimulation condition is chosen to be 1 mA, 1-10 V square wave, 1.0 to 2.0 ms pulse duration at 30 Hz.

3.2. System Overview

The implantable wireless system is composed of the implantable wireless device and base station. Similar to the skin-mountable recording device, the implantable device is composed of Bluetooth SoC, recording circuit with filtering stage, and stimulator. The overall high-level overview of the system is shown in Figure 3.2.

The recording circuit of the implantable device is different from that of the skin-mountable device for overall gain and passband. The recording circuit consists of an INA333 for the instrumentation amplifier and an OPA333 for the filter and non-inverting gain stage. As the signal measured at the pelvic nerve is in the microvolt range, the gain should be very high. The final gain of 20,000 is achieved with initial gain of 100 at pre-amplifier (INA333) and non-inverting operational amplifier with the gain of 200.

The filter topology is Sallen-Key and the magnitudes of the capacitor and resistors are chosen to produce a passband from 30Hz to 3kHz. As there is strict limitation in terms of physical dimension of the device, recording differential input of EUS-EMG signal is achieved with two cuff electrodes to minimize the overall dimensions of the device.

The stimulation part is composed of a single non-inverting operational amplifier (TLV2471-Q1, Texas Instruments) and Bluetooth SoC (nRF51822, Nordic Semiconductor). Bluetooth SoC is composed of multiple general-purpose input/output (GPIO) channels that can be programmed to produce output based on the pulse width modulation (PWM). One GPIO is programmed to produce a stimulation signal of 3 V square wave with 1.0 ms pulse duration at 30 Hz. The signal is further amplified through the non-inverting operational amplifier to produce 6 V square wave output.

A smartphone with BLE connectivity is used as the base station. Unlike the skin-mountable wireless system, the base station here in the implantable system serves as both receiver and transmitter. As a receiver, it receives the recorded electrophysiological signal of the pelvic nerve from the wireless device. In addition, it also transmits a command to the device to control the stimulation event. The GUI for the base station is shown in Figure 3.3. The GUI is composed of a recording subpart with a waveform and a stimulation subpart with a command window. Typing alphabet letter ‘g’ in the command window starts the stimulation, while typing ‘s’ stops the stimulation. In both recording and stimulation modes, the connection button is used to connect the Bluetooth device or to

disconnect from it.

3.3. Design Considerations

3.3.1. Implantable Wireless Device Firmware

The implantable wireless device uses the same BLE SoC (nRF51822) as in the skin-mountable wireless device, but the firmware flow is different as it controls both transmitting (TX) and receiving (RX) events. The internal ADC is configured with 8-bit conversion at 1 kHz sampling rate. The EUS-EMG signal is then digitized through this ADC and the result is transmitted through Bluetooth radio to smartphone. The firmware flow is shown in the Figure 3.4.

The 2.4 GHz radio power is chosen to be 0 dBm. The optimum radio power is determined by measuring the received signal strength indication (RSSI) level at one meter away from the wireless device in air and phosphate buffered saline (PBS) solution (Sigma-Aldrich, 0.01M, pH 7.4 at room temperature). The PBS solution is used to provide a test environment similar to the human body as it has matched osmolarity [12]. Thus, the PBS solution is used as a reference model to find the optimum radio power. For this measurement, wireless devices configured with different radio power levels are prepared and passivated with polydimethylsiloxane (PDMS). Then, the RSSI levels of these devices are measured in air at 1 meter away, followed by a second measurement after being immersed in PBS solution. The result is shown in Table 3.1, showing that there is a slight degradation in signal strength in PBS solution compared to the operation in air. To ensure the optimum operation of the device with

significantly strong signal strength after implantation, the radio power level needs to be chosen higher than that for the skin-mountable device. Therefore, the radio power is chosen to be 0 dBm to compensate for the degradation in the implantable device.

3.3.2. Recording and Stimulation Circuit

The recording circuit of the implantable device, shown in Figure 3.5, is almost identical to that of the skin-mountable device, shown in Figure 2.5. One of the differences is the values of the components in the filter stages to make the passband between 30 Hz and 3 kHz. Also, the overall gain of the recording circuit is 20,000, which is to satisfy the higher demand due to weaker signal at the pelvic nerve, compared to EMG signal. In Figure 3.6, the frequency response of the implantable device is shown. The overall gain within the passband is about 86 dB, which is 20,000 in voltage level. The cutoff frequencies of low-pass and high-pass filters are chosen at 30 and 3 kHz, respectively, at the gain of approximately -3 dB. Rather than these differences, the recording circuit performs the identical function as in the skin-mountable device.

The stimulation is achieved either electrically or optically. The electrical stimulation is achieved with generated pulse from Bluetooth SoC (nRF51822) via non-inverting operational amplifier with gain of two. The pulse width and amplitude of the stimulation signal are chosen based on the previous system requirement, described in Section 3.1. The output is connected with a cuff electrode that is directly attached to the pelvic nerve to induce the stimulation. The optical stimulation is achieved by controlling the μLED. According to researchers in the field of optogenetics, a light with specific wavelength can

control neuronal activity of a nerve [13]. Likewise, the stimulation circuit makes use of blue light (475 nm) at 10-30 Hz frequency to activate Advillin-ChR2 sensory neurons to induce contraction of bladder and red light (632 nm) to deactivate it. In this way, the bladder activity during stimulation can be distinguished from natural bladder activity. The schematic of the stimulation circuit is shown in Figure 3.7.

3.3.3. Cuff Electrode

The cuff electrode was designed and developed by collaborators, Dr. Gunchul Shin and Dr. Jangyeol Yoon, but it is introduced and explained here as it is an important part in the overall system. In Figure 3.8, the representative model of cuff electrode is shown. As the pelvic nerve of a female rat is hard to penetrate and there is very limited space available for the electrodes, the cuff electrodes need to be thin and flexible. These mechanical properties are achieved by using thin PDMS layer as a substrate (500 μm) and top cover (200 μm). The cuff electrode also consists of an optical stimulator with μLEDs. The modulus of the cuff electrode is around 10 kPa, which is low and soft enough to be implanted without damaging the pelvic nerve.

The cuff electrode implantation model is shown in Figure 3.9. Here, a thin bar is used to mimic the pelvic nerve to show that the cuff electrode is fabricated with the right dimensions to match those of the pelvic nerve. In addition, the impedance result of the metal electrode as a function of frequency indicates that the metal electrode fabricated with platinum (Pt), gold (Au), and chrome (Cr) has an impedance in the kilohm range.

Figure 3.10 shows a photograph of the actual implantation of the cuff electrode at the pelvic nerve during *in vivo* testing. The cuff electrode, with its flexibility and effectively low modulus, easily penetrates beneath the fragile and small pelvic nerve near the bladder, indicating minimal risk at the neural interface during *in vivo* experiments.

3.3.4. Power Consumption

The power consumption of the implantable device is described in Table 3.2 and Table 3.3 during TX and RX events, respectively. The RX event requires more power as the radio consumes more current. A 16 mA current at operating voltage of 3 V implies that the device needs a battery with significant capacity, while the space available limits the capacity of the battery greatly. It is not an ideal situation to replace the battery after implantation. In addition, it is not possible to either reduce the power consumption further or use a large battery for long operation. Therefore, the possible solution is to have a wireless powering scheme. The wireless charging station is discussed in Chapter 4.

3.4. Figures

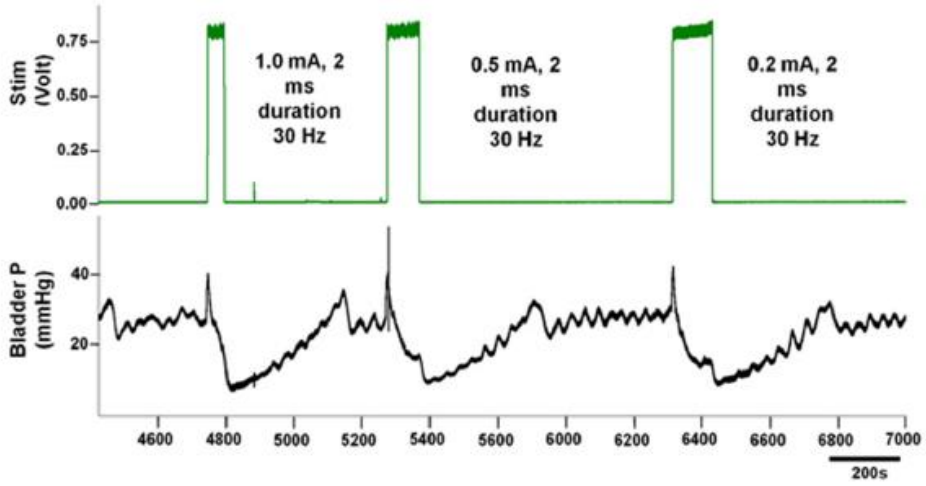

Figure 3.1: A representative figure showing bladder pressure response at three different stimulation conditions: 1.0, 0.5, and 0.2 mA for 2ms at 30 Hz. Reduction in bladder pressure is shown in all cases. Stimulation experiment is performed with cuff electrode and pulse is generated in a pulse generator. This data is acquired by Yee Hsee Hsieh at Case Western University, a collaborator of this project.

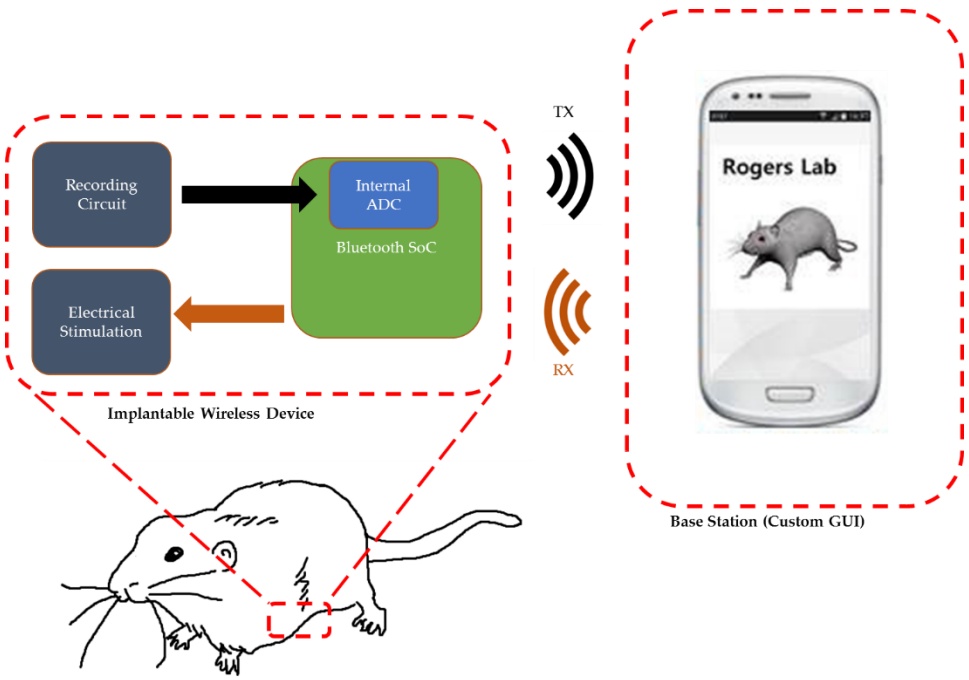

Figure 3.2: A high-level overview of the implantable wireless recording and stimulation system composed of the implantable wireless device and base station: 1) implantable device for recording EUS-EMG signal, applying stimulation, and transmitting recorded signal, 2) base station controlling stimulation of the device and receiving recorded EUS-EMG signal at pelvic nerve.

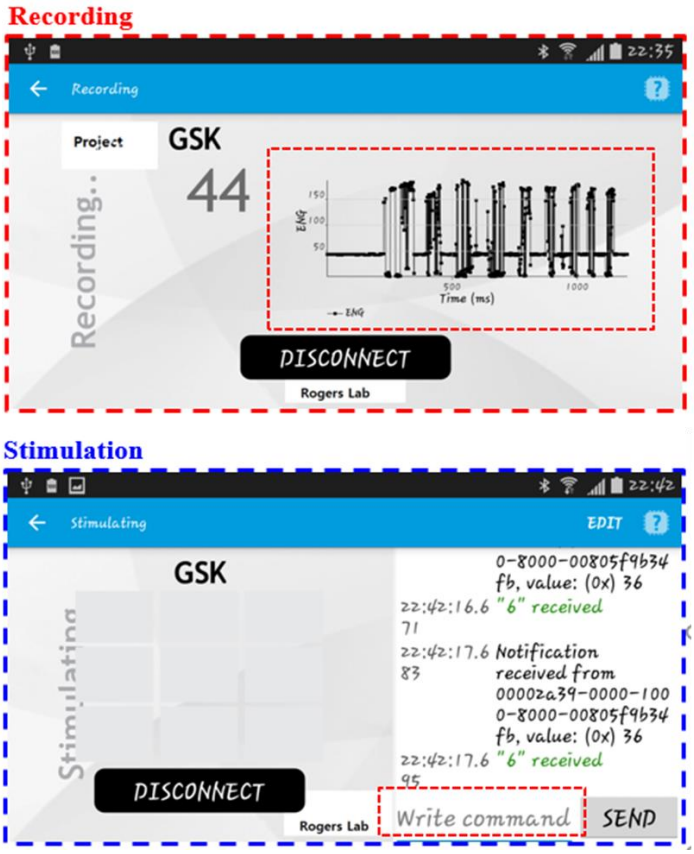

Figure 3.3: Android based smartphone GUI for recording (top) and stimulation (bottom).

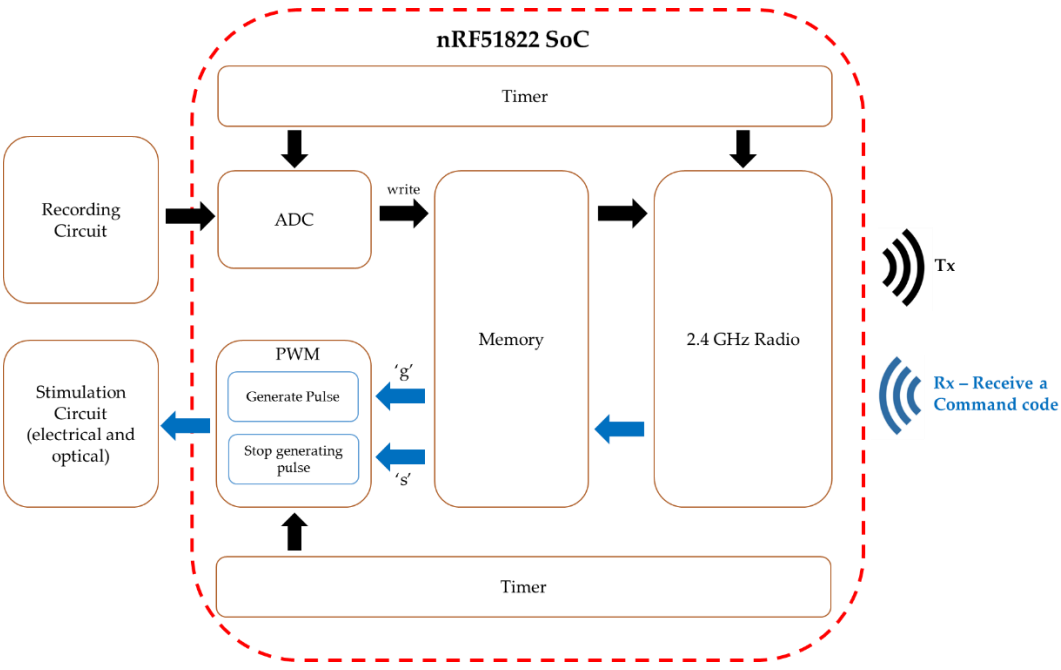

Figure 3.4: High level overview of firmware controlling the implantable wireless device.

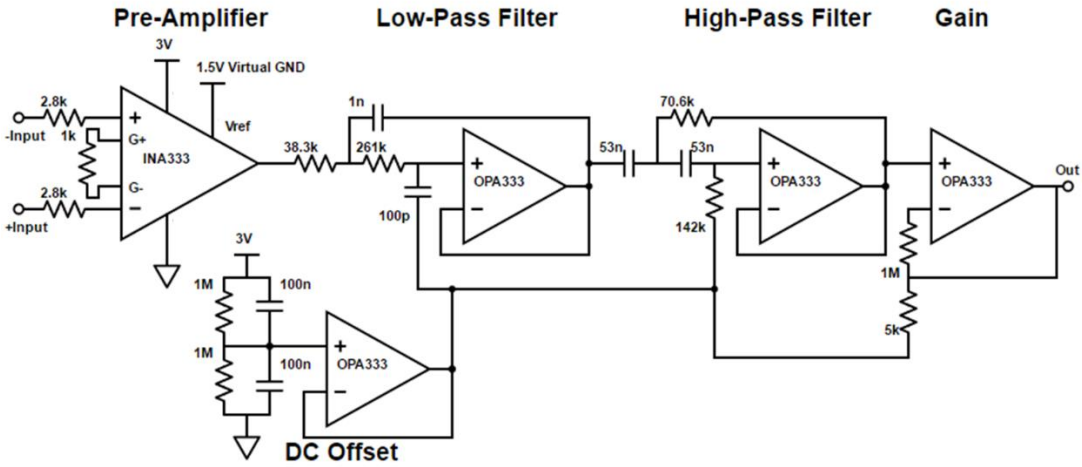

Figure 3.5: The schematic of the recording circuit of the implantable device.

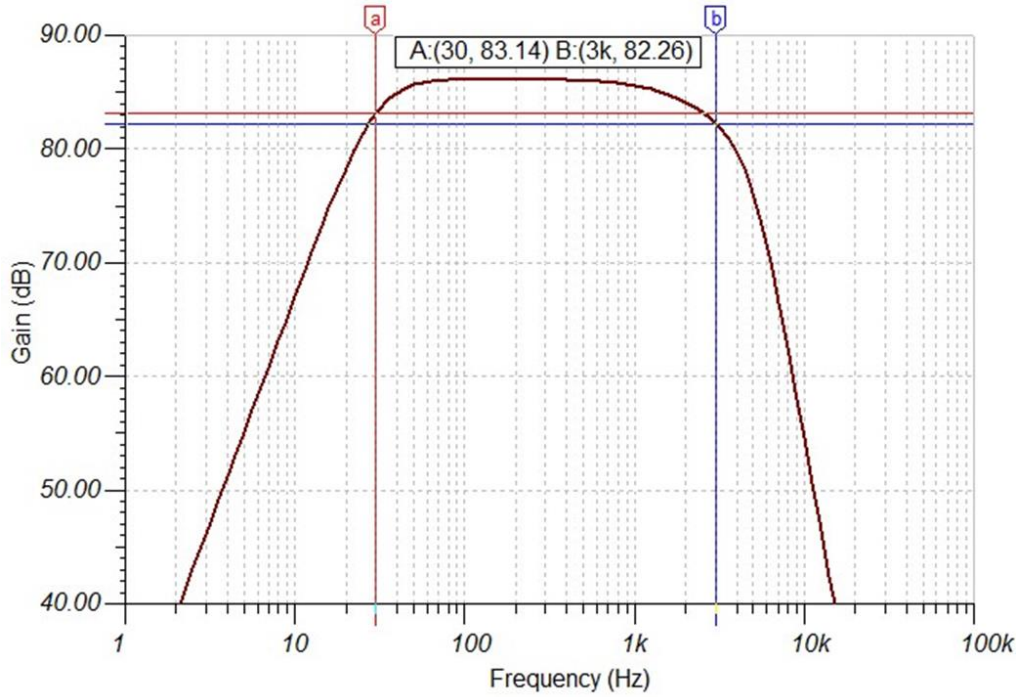

Figure 3.6: The frequency response of the implantable device.

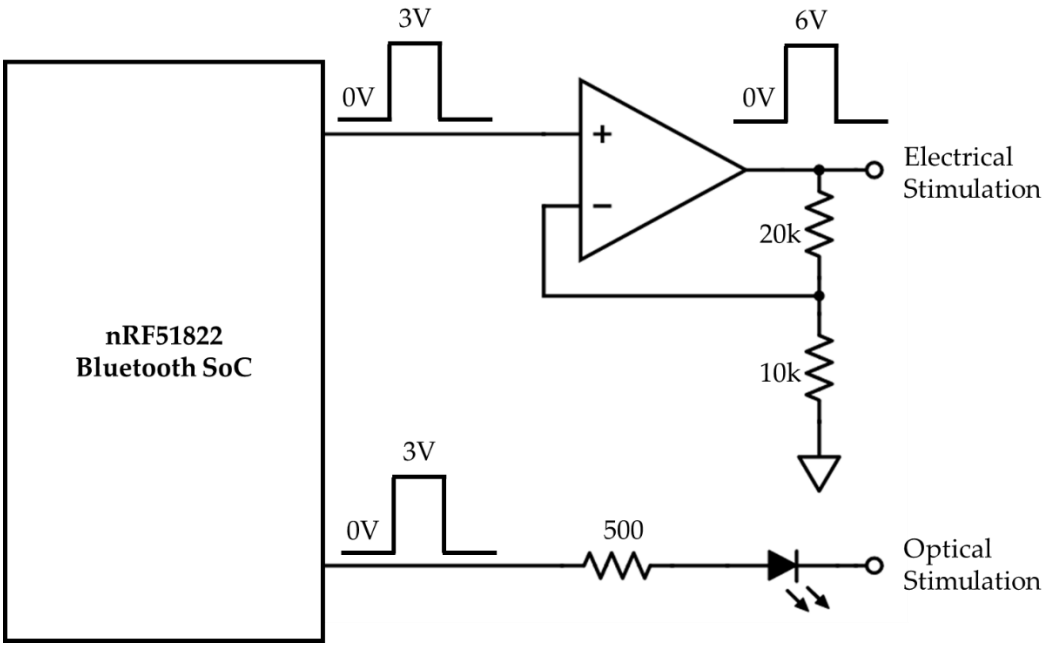

Figure 3.7: The schematic of the stimulation circuit of the implantable device.

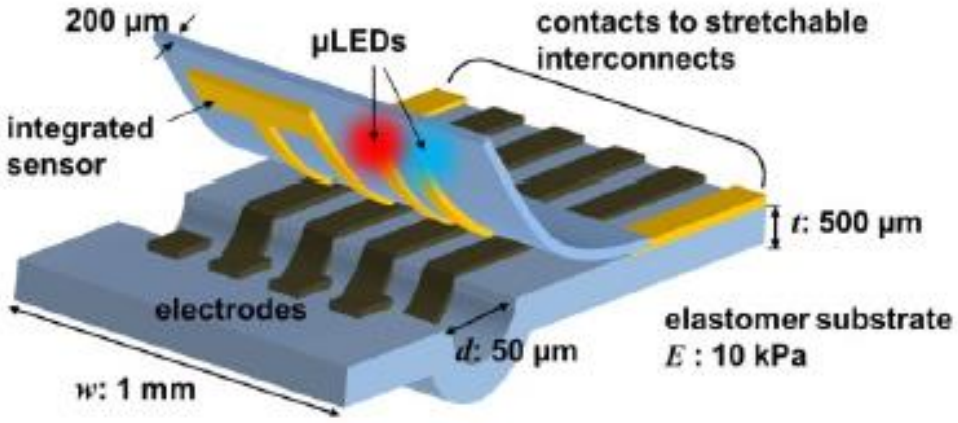

Figure 3.8: The representative model of cuff electrode composed of four electrodes for differential recording and electrical stimulation and optical stimulator with micro LEDs. The cuff electrode is covered with thin PDMS.

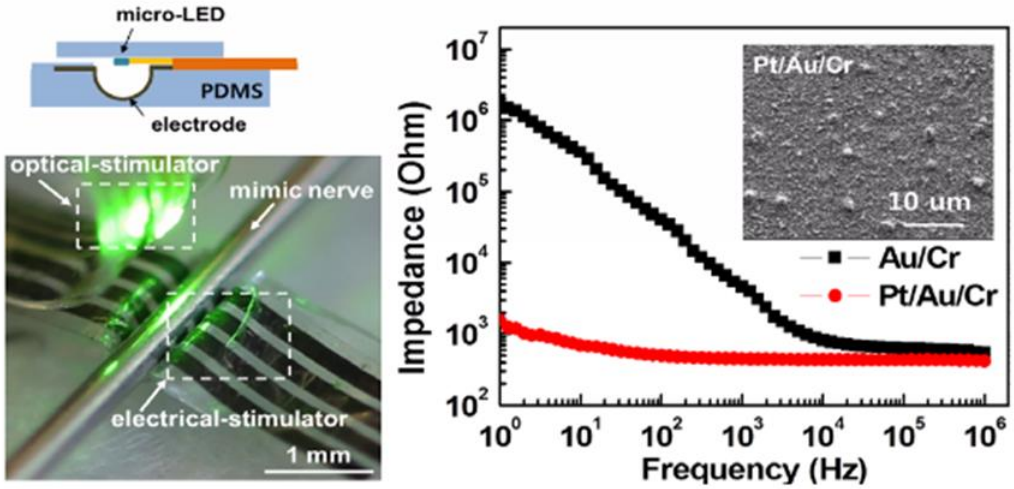

Figure 3.9: The cuff electrode implantation model with mimic nerve as a thin bar with optical stimulator attached (Left). The plot displays the relationship between impedance and frequency in two different metal composition: Au/Cr and Pt/Au/Cr. These figures and images are created by Dr. Jangyeol Yoon.

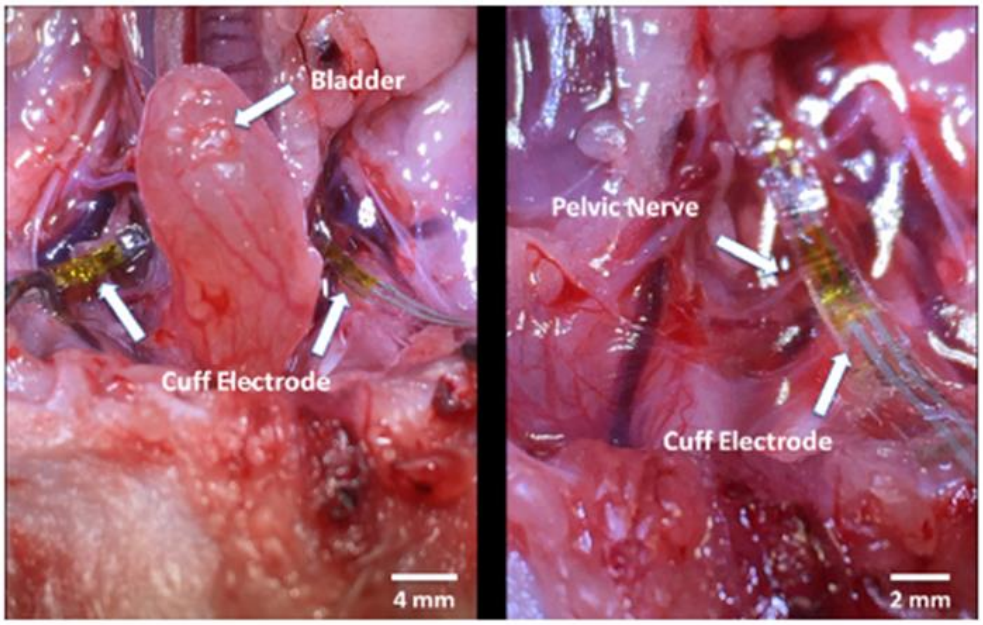

Figure 3.10: The real image of implanted cuff electrode in a female rat at the pelvic nerve. The picture clearly shows the bladder and pelvic nerve and it is obtained by collaborators in Prof. Gereau group at Washington University in St. Louis.

3.5. Tables

Table 3.1: RSSI level comparison between in-air and in-PBS solution indicating RF properties of wireless device inside a rat.

TX Power (dBm)	RSSI Level (dBm) in air	RSSI Level (dBm) in phosphate buffered saline (PBS)
+4	-56	-61
0	-60	-66
-4	-66	-70
-8	-71	-77
-12	-76	-82

Table 3.2: The current consumption of the implantable device during TX event.

Components		Current Consumption (mA)
NRF51822 SoC [9]	CPU	2.4
	Radio at 0 dBm	10.5
	ADC	0.26
Instrumentation Amplifier		0.05
OP AMP x 2		0.034
Total Current Consumption		13.244

Table 3.3: The current consumption of implantable device during RX event.

Components		Current Consumption (mA)
NRF51822 SoC [9]	CPU	2.4
	Radio at 1 Mbps	13
	ADC	0.26
OP AMP		0.6
Total Current Consumption		16.26

CHAPTER 4: A Wireless Power Charging Station

This chapter introduces a wireless power charging station to energize the implantable device by recharging a small rechargeable battery, which is the primary power source of the implantable device. The wireless charging station secures the robust and continuous operation of the device after implantation by providing enough power at around 62 mW.

4.1. Design Considerations

The inductive power link is established at frequency of 13.56 MHz for its negligible effect on human tissue [14]. In addition, the prototypical inductive link is built with our collaborator's existing transmitter coil by Feig Electronic with dimensions of 31.8 cm x 33.8 cm (L x W), operating at 13.56 MHz [15]. A reader module by Feig Electronic provides an auto-tuning function and configures the coil to transmit at a power level up to 4 W [16].

The inductive link needs to provide enough power at reasonable range. As the implantable device requires about 50 mW, the link should provide no less than that. In addition, the optimum range should cover at least the height of a rat, which implies that the range needs to be at least 5 cm. In addition, the coil dimensions of the receiver cannot be larger than 3.0 cm x 3.0 cm (L x H) due to space limitation.

4.2. Inductive Power Link

The schematic of the inductive power link with parallel resonant tank at the receiver side is in Figure 4.1. The parallel resonant tank, formed by adding a capacitor to tune the resonant frequency of 13.56 MHz, is used to achieve the highest power transfer, because the inductive link without resonant tank usually suffers from leakage inductance and low coupling coefficient [17]. The inductive link can be analyzed with circuit theory, which models the transmitter coil and receiver coil in terms of voltage source and passive components as shown in Figure 4.1. The resonant frequency can be found by the Equation (4.1).

$$\boldsymbol{f_0 = \frac{1}{2\pi\sqrt{L_1 C_1}} = \frac{1}{2\pi\sqrt{L_2 C_2}}} \tag{4.1}$$

The analysis of the schematic, shown in Figure 4.1, can be simplified significantly by applying the reflected impedance concept and the procedure given in the literature [18]. The equations of the reflected impedance, efficiency, and the delivered power to the load are written in Equations (4.2), (4.3), and (4.4), where $k_{12} = M_{12}/(L_1L_2)^{0.5}$, $Q_1 = \omega_0 L_1/R_1$, $Q_2 = \omega_0 L_2/R_2$, $Q_L = R_L/(\omega_0 L_2)$, and $Q_{2L} = Q_2 Q_L/(Q_2+Q_L)$ [18].

$$\boldsymbol{R_{ref} = k_{12}^2 R_1 Q_1 Q_{2L}} \tag{4.2}$$

$$\boldsymbol{\eta = \frac{k_{12}^2 Q_1 Q_{2L}^2}{(1 + k_{12}^2 Q_1 Q_{2L}) Q_L}} \tag{4.3}$$

$$\boldsymbol{P_L = \frac{V_s^2 k_{12}^2 Q_1 Q_{2L}^2}{2R_1(1 + k_{12}^2 Q_1 Q_{2L})^2 Q_L}} \tag{4.4}$$

Optimization of the inductive link can be achieved by using the Equations (4.1) - (4.4). However, the constraint of using the existing transmitter coil is that the parameter on transmitter side is unknown. Therefore, the simulating parameters are not an ideal option. Rather,

the strategy here is to get an idea from real experiments and to make use of the large power transmitted by the transmitter module, which can provide a power level up to 4 W. The coil dimensions are chosen to be 3 cm x 3 cm with single-turn as a prototype. The parameter including inductance of the coil, measured by a RF impedance analyzer (4291A, Hewlett Packard), is 121 nH at 13.56 MHz. The tuning capacitor is then chosen to be 1100 pF based on Equation (4.1) for resonance tuning. Figure 4.2 shows the prototype made of 22 AWG wire on the breadboard for the initial experiment. The peak-to-peak voltage is then measured at the 300 Ω resistor. When the voltage is measured, the LED is disconnected and replaced by the 300 Ω resistor. The result is that the delivered power level is about 62 mW with the Vpk of 4.33 V at a distance of 5 cm from the transmitter. Figure 4.3 shows the implanted model and setup for wireless power transfer. The result indicates that the receiver coil in this dimension can deliver enough power to the device. Therefore, the dimensions of the coil are chosen as 3 cm x 3 cm (L x W).

The coil in the implantable device is made of copper fabricated using standard photolithography process and is shown in Figure 4.4. The AC power obtained is then further processed through the full-wave bridge rectifier with smoothing capacitor and low dropout regulator (LDO). During the full-wave bridge rectifier, the Schottky diode is being used because of its lower voltage drop compared to a silicon diode. The overall receiver circuit model is illustrated in Figure 4.5. The full-wave rectifier operates such that diodes D1 and D2 conduct during the positive half-cycle while diodes D3 and D4 conduct during

the negative half-cycle. The resulting receiver was verified to successfully deliver enough power to the implantable device by enabling all the functionalities designed for the implantable experiments, thus making the wireless charging scheme applicable.

4.3. Figures

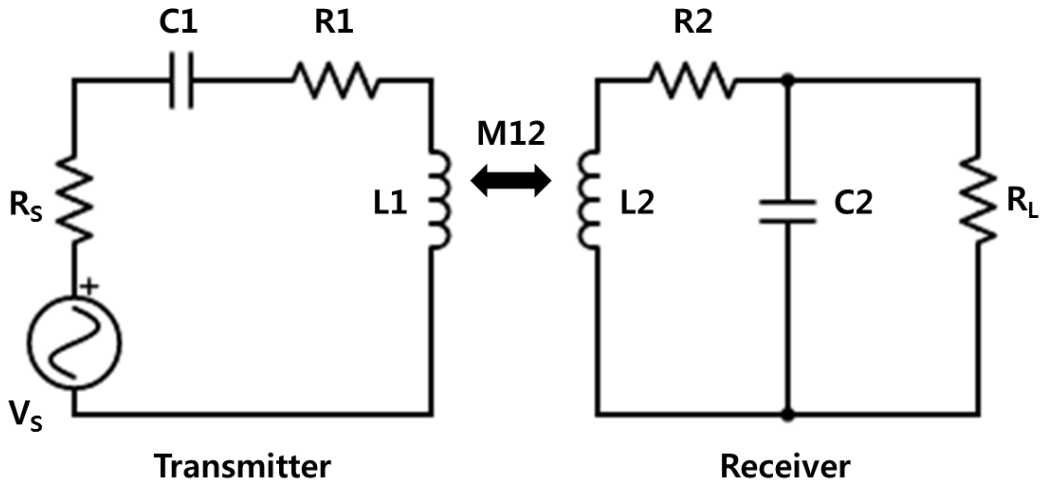

Figure 4.1: The schematic of inductive link with parallel resonant tank at receiver coil.

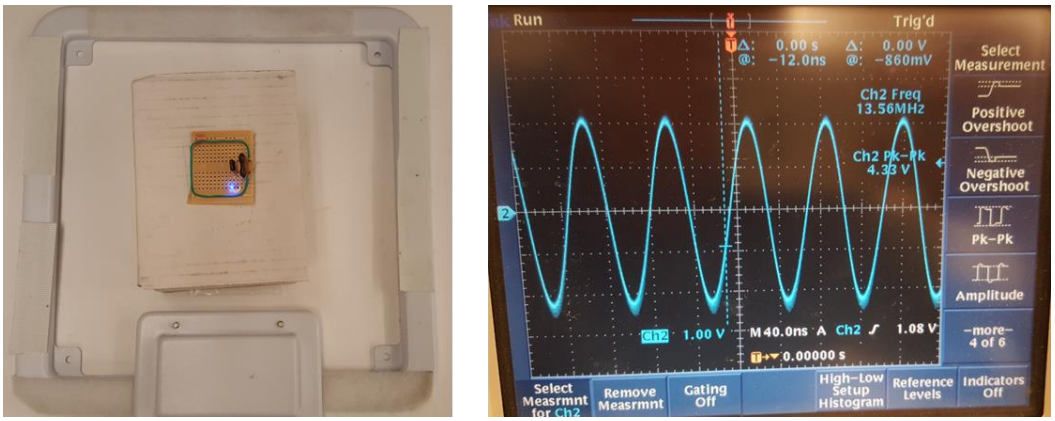

Figure 4.2: Receiver coil made of 22 AWG wire with tuning capacitor and blue LED connected, placed on the 5 cm height box around transmitter coil (Left). Peak-to-peak voltage response measured on the resistor of 300Ω connected instead of the LED as 4.33 V exceeds the maximum rating of a blue LED (Right).

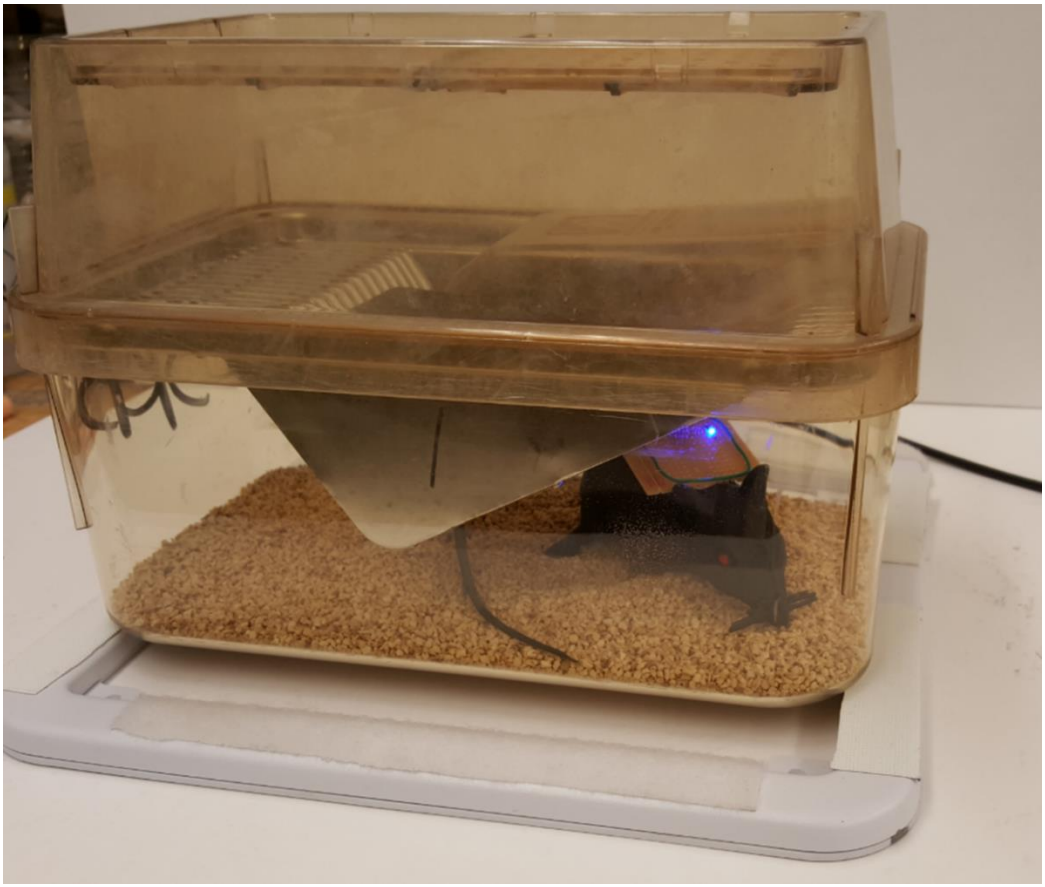

Figure 4.3: The implanted model consists of a toy mouse inside a cage, transmitter coil, and the receiver.

Figure 4.4: The inductive coil made of copper using photolithography, compatible functionality to the coil made of AWG wire.

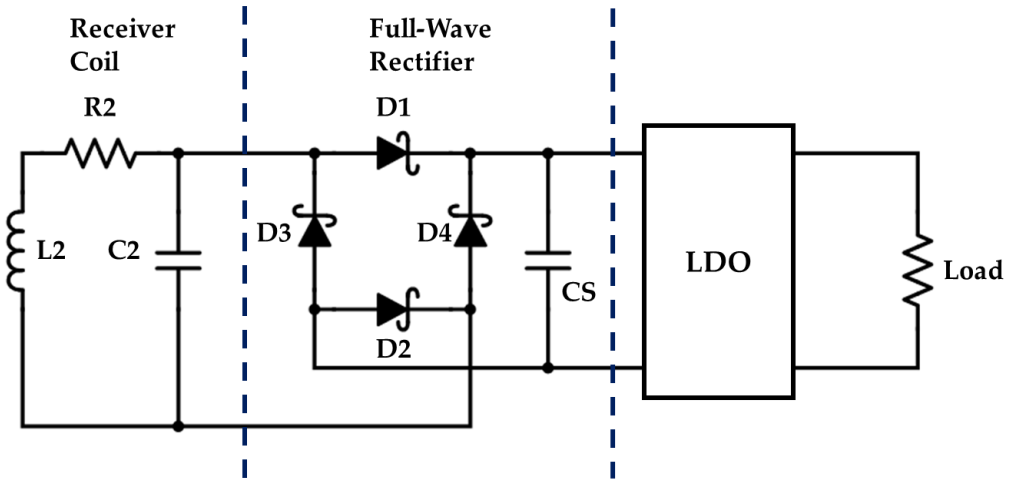

Figure 4.5: The schematic of the receiver with full-wave rectifier with smoothing capacitor (CS), LDO, and the load.

CHAPTER 5: Results and Discussion

5.1. Skin-mounted Experiments

The skin-mountable wireless recording system has been validated with experiments on skin. The picture of the device is in Figure 5.1. The device is placed on the skin and measures sEMG and acceleration signal associated with movement of the forearm. The overall dimensions of the system are 3 cm x 3 cm including fabricated electrodes of 0.7 cm x 1 cm (L x W) and three batteries of 9.5 mm diameter x 1 cm height.

In Figure 5.2, the sEMG signal is displayed. This is the sEMG signal through gain and filter stage and transmitted wirelessly after being digitized. The result shows a clear response to periodic clenching and relaxing a fist. The baseline is set at 1.5 V to fully extract the signal variation from 0 to ± 1.5 V with single DC supply operation (+3 V to GND) and it is clearly shown in Figure 5.2. In addition, the range of signal variation is chosen with the right amount of gain to prevent saturation of amplifiers, where the saturation occurs at 3 V. The result confirms that the signal variation is within the saturation limit.

In Figure 5.3, the signal from the 3-axis accelerometer is displayed. The result clearly shows the response due to intentional shaking. It shows a large change in all of the x, y, and z axis signals during vibration of a forearm. When the forearm is still and relaxing, the signal shows very small variations in all of the x, y, and z axes.

5.2. Fully Implanted Experiments

The implantable wireless device is shown in Figure 5.4. The device is passivated by soft polymer (PDMS). It is stretchable and flexible with the flexible substrate and stretchable metal interconnects as shown in Figure 5.4. The boundary of the device is filled with inductive coil for wireless power transfer. Here, the inductive coil is copper layer fabricated such that the functionality is compatible with the coil made of AWG wire in Chapter 4.

The EUS, EMG, and bladder pressure data, acquired with the cuff electrode described in Section 3.3.3, is shown in Figure 5.5. This is measured in wired fashion merely to demonstrate the functionality of the cuff electrode. Continuous cystometrograms (CMGs) with saline infusion (6ml/h) are collected to capture bladder function during voiding and filling. The result clearly shows changes in EUS, EMG, and bladder pressure during voiding and filling.

The result in wireless mode is illustrated in Figure 5.6. It shows that the implantable wireless device can acquire a result similar to that of the wired mode. The bladder pressure is measured with a pressure transducer, which is not involved in the design of the implantable system. The response measured at the pelvic nerve matches the bladder pressure in both wired and wireless mode, indicating that the wireless device operates in the desired manner.

The stimulation result is shown in Figure 5.7. The Android GUI

controls stimulation of the implantable wireless device and the stimulation conditions are 6 V for 1 ms at 20 Hz. A pressure transducer, attached to the bladder, measures the bladder pressure response. The black box in the right plot of Figure 5.7 illustrates the pressure change during natural voiding of the bladder and the red box illustrates the change associated with the stimulation. The result shows that the pattern of pressure change is similar in both natural and stimulated voiding, indicating that the system is capable of monitoring bladder activity associated with external stimulation.

5.3. Figures

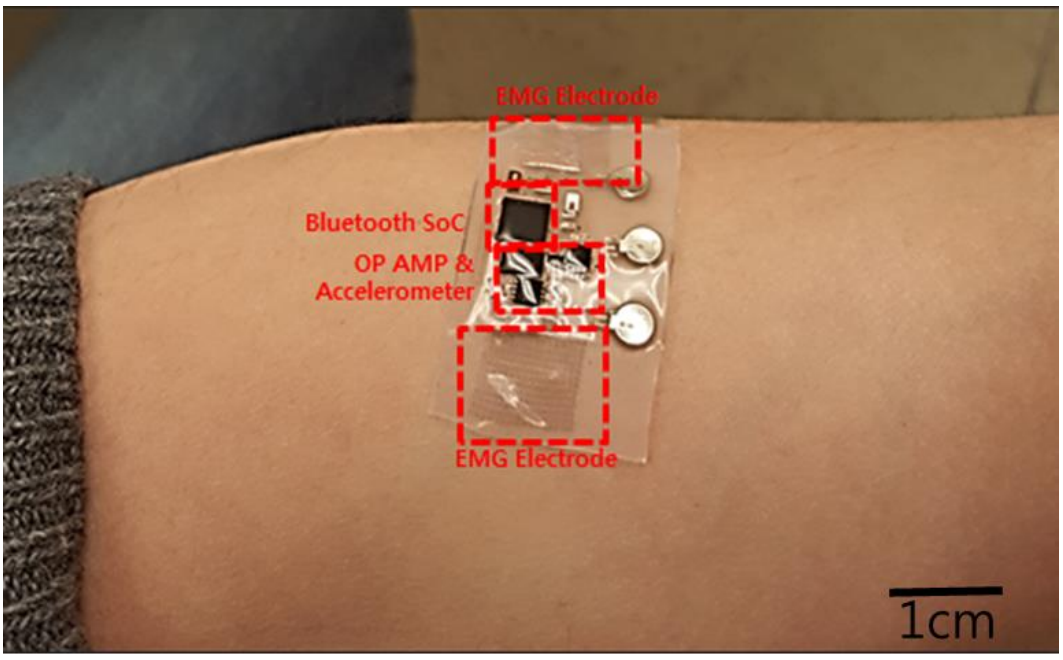

Figure 5.1: The representative image of the skin-mountable device composed of Bluetooth SoC, recording circuit, batteries, and surface electrodes.

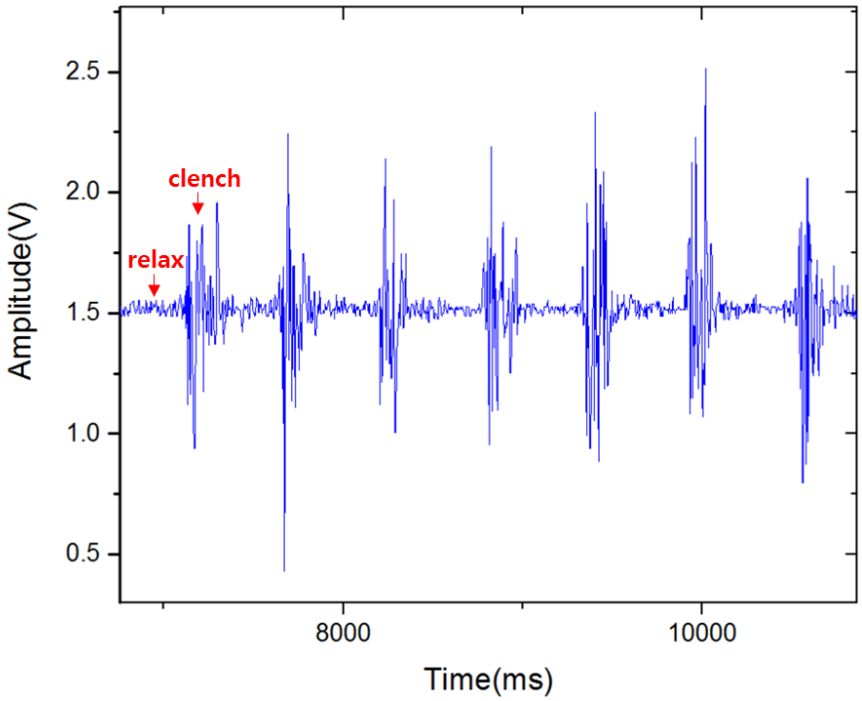

Figure 5.2: sEMG data showing different response during relax and clench of forearm.

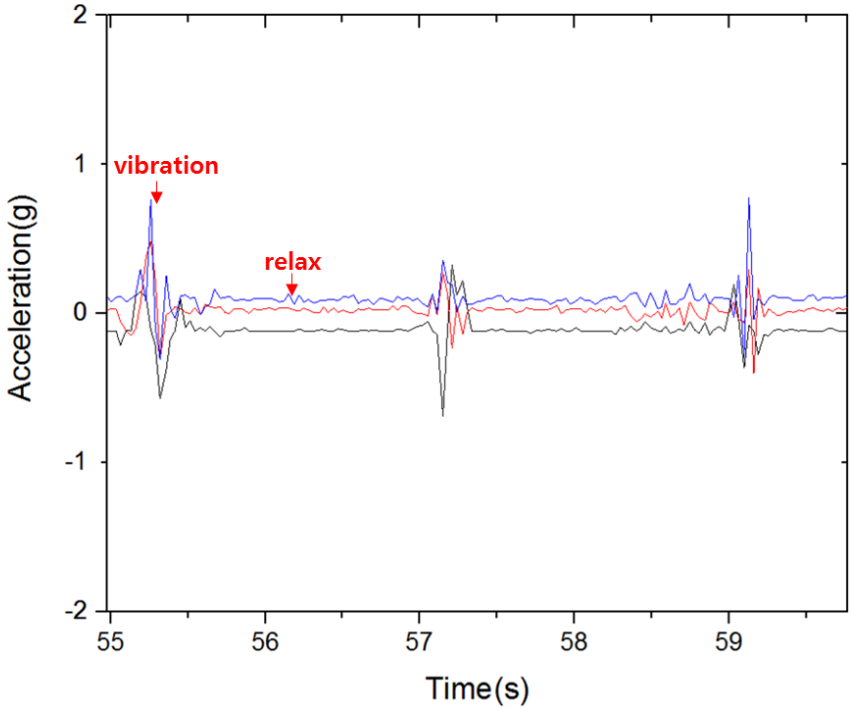

Figure 5.3: Acceleration data acquired during vibrating and relaxing a forearm.

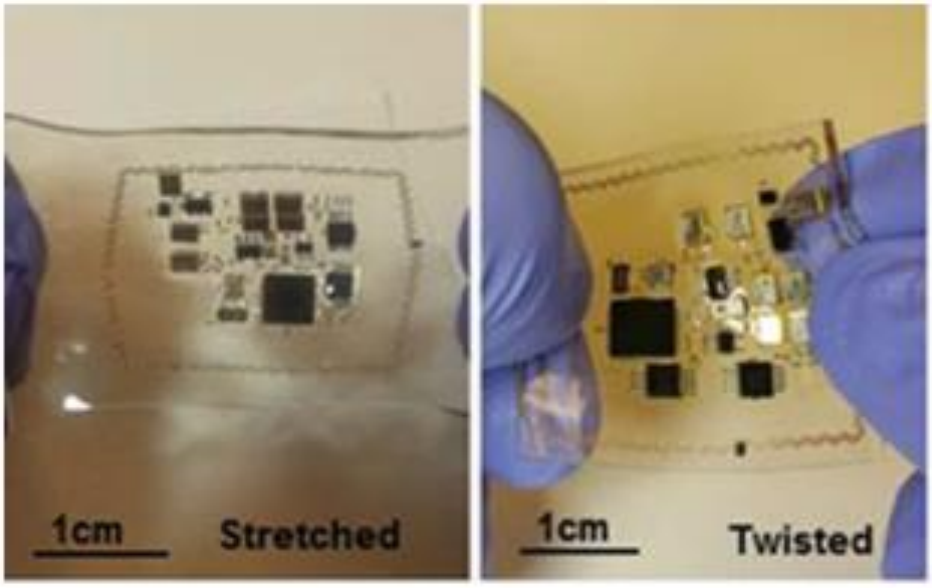

Figure 5.4: The implantable device without cuff electrode being connected in stretched (Left) and twisted (Right) view to demonstrate stretchability and flexibility.

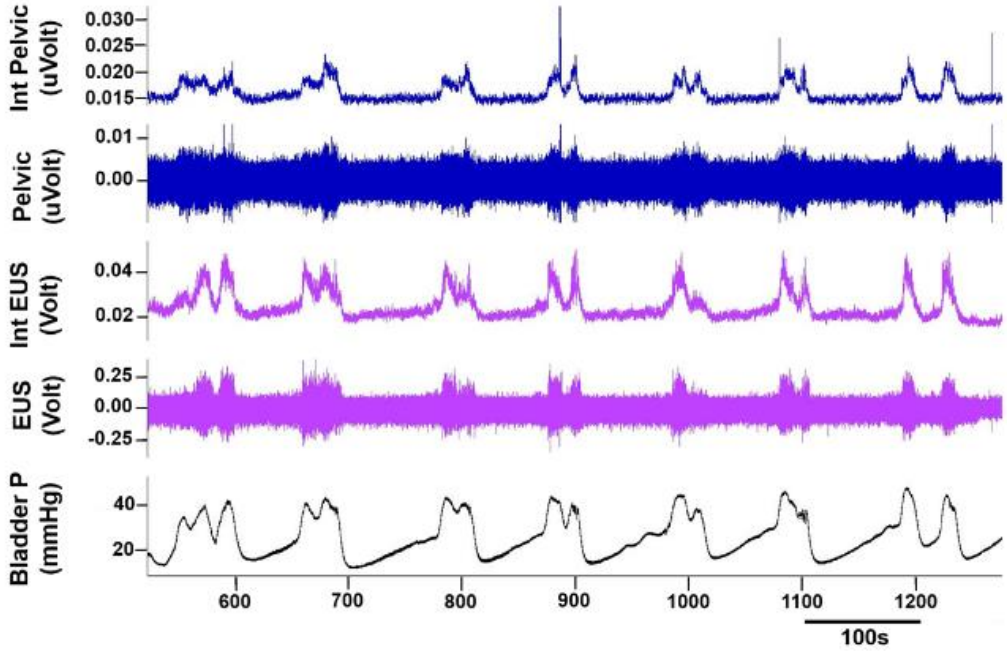

Figure 5.5: The representative results acquired with neural interface with fabricated cuff electrode. This data is measured in wired communication with the cuff electrode to demonstrate the functionality of the cuff electrode.

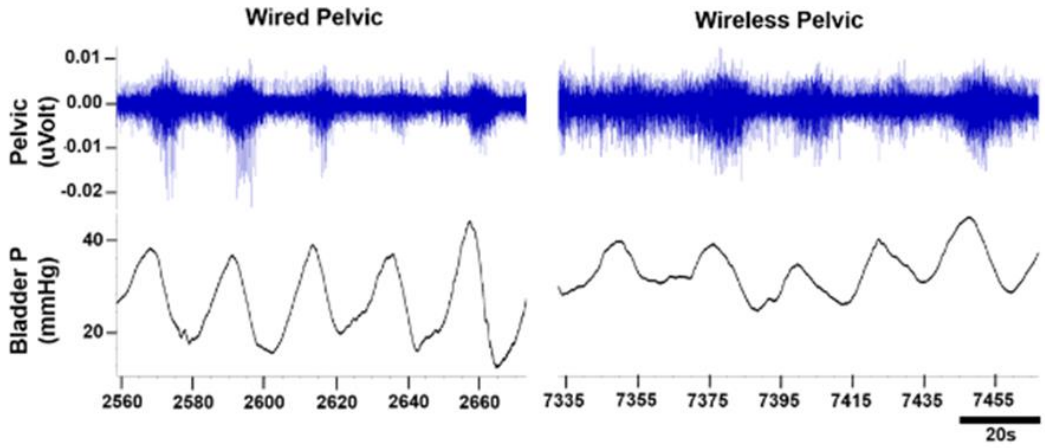

Figure 5.6: Comparison between wired recording (Left) and wireless recording (Right) at pelvic nerve. The data was acquired by Yee Hsee Hsieh

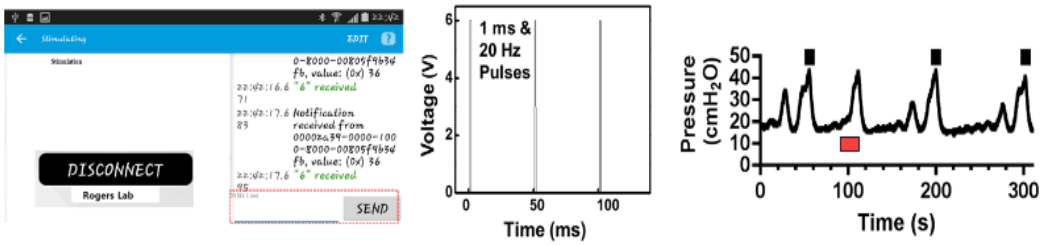

Figure 5.7: The representative results showing pressure change (Right) in wireless electrical stimulation (Middle) controlled by Android application GUI (Left). The black represents bladder pressure in natural voiding and the red box is when the voiding occurs by wireless stimulation.

CHAPTER 6: Conclusion

In this thesis, a soft, stretchable, and wireless biomedical recording system has been explored. The skin-mountable device can achieve a continuous monitoring of sEMG signal and acceleration of forearm with flexibility and stretchability. In addition, the system achieves an effective wireless communication with the range of a few meters. With its miniaturized dimensions of 30 mm x 30 mm x 1.5 mm, the power budget is up to 3 hours with a 33 mAh battery. With slightly larger dimensions, the power budget can be significantly increased with more battery capacity. Thus, the dimensions and battery life should be carefully chosen depending on the specific applications.

The implantable device is capable of recording an EUS-EMG signal with a cuff electrode designed to penetrate under a pelvic nerve of a female rat. The gain and frequency filtering is determined appropriately to produce reasonable results. In addition, the device can stimulate the pelvic nerve to monitor the bladder activity either electrically or optically. The wireless power charging station ensures continuous operation after implantation by providing power level of 62 mW, which is enough for the implantable device. Therefore, the overall system with additional power source, acquired by a wireless charging station, can effectively record EUS-EMG signals and stimulate the pelvic nerve while the base station can control receiving and transmitting wirelessly.

The next step for the skin-mountable device is to make use of developed devices in the clinical studies such as tremor detection. In addition, various other electrophysiological signals such as ECG can be measured with slight modifications in the device so that broad applications are accessible. In addition, the skin-mountable platform can be improved in terms of mechanical robustness by developing a unique microfluidic enclosure method, similar to the soft platform demonstrated by Xu et al. [3]. Establishing a sensor network with chip-to-chip communication enabled by a star topology is also an interesting idea as the next step.

The implantable device can be improved in multiple aspects. First, the current design does not include a pressure transducer in the implantable platform. Making the pressure transducer in miniaturized and implantable fashion will finalize the design of the implantable device for bladder activity monitoring. Second, the wireless charging station can be improved further to provide battery-less operation. Currently, the use of the existing transmitter module significantly limits the design parameters on the transmitter side. Developing a transmitter module with a Class-E amplifier and optimized coil dimensions for this application will give more freedom in designing an effective inductive link. Third, the multi-coil approaches can be studied to improve the efficiency. Studies have shown that the 3- or 4-coil magnetic resonant system can yield significant improvements in efficiency [19, 20].

In conclusion, the developed wireless biomedical electronics system can be

used in both skin-mountable and implantable applications. These devices provide portability and a user-friendly environment with the wireless communication mode. In addition, the devices have great potential and broad implications for clinical studies.

APPENDIX: Fabrication and Mechanical Properties

The uniqueness of this recording system also comes from its mechanical properties with the soft and stretchable platform. The softness is achieved by passivation with silicon based soft polymer, either PDMS or Ecoflex. Ecoflex is a soft and stretchable silicon elastomer, while Ecoflex is known as a softer material than PDMS. The side view of the system and CAD layout for stretchable electrodes and system are shown in Figure A.1. It has been reported in many studies that a high stretchability can be achieved with a serpentine pattern on a flexible elastomer substrate [3], [21], [22]. In addition, it has been reported that the soft and stretchable platform is particularly useful for implantable systems when the target organ or tissue is hard to study with a rigid system [13]. Thus, the design follows the methodology that has been developed from past studies to achieve high flexibility and stretchability.

The wire interconnect is designed to stretch up to 20 percent. The stress associated with stretching should be minimized so that the wire can be stretched and recovered back and forth multiple times without mechanical deformation. In the Figure A.2, the simulation result of the stress profile, while a stretching the wire by 20 percent, is illustrated. The wire fabricated based on this simulation result has been validated with more than 100 of stretches without deformation.

The fabrication procedure is described in Figure A.3. First, a glass slide as a sacrificial substrate is prepared and coated with PMMA with spin coating

(3000 rpm, 30 seconds) followed by soft bake (180 °C, 2 minutes). The PMMA layer prevents bonding between glass slide and Ecoflex. Second, Ecoflex is spin coated on PMMA (500 rpm, 30 seconds) and cured at room temperature for 4 hours (Figure A.1 (b)). Third, a separate glass slide is prepared and coated with PMMA. Then, SiO_2 (100 nm) is deposited by e-beam evaporation. Polyimide is spin coated (3000 rpm, 30 seconds) and cured in an oven (250 °C, 1.5 hours). Then, a Cr/Au (5 nm/2 μm) layer is deposited by e-beam evaporation followed by photolithography and wet chemical etching for the system layout pattern as in Figure A.1 (c). Another polyimide layer is spin coated and cured. Polyimide layers are directly etched away by reactive ion etching (March RIE, 300 mTorr, 200 W, 20 sccm of O_2, 20 minutes) to open the contact pad and stretchable interconnect. These separately prepared layers are transfer printed onto initial glass slides with an Ecoflex layer. In this step, water soluble tape picks up the stack layers after the PMMA layer is removed with acetone. Here, Ecoflex and SiO_2 form a strong bond. Then, IC components and passive components like resistors and capacitors are soldered. Finally, the fabrication is complete after spin coating Ecoflex on the top layer. The thickness of the Ecoflex layer is about 100 μm and that of the system with layers of polyimide and Cr/Au is about 1.1 mm. Therefore, the overall thickness is about 1.3 mm. The fabrication procedures for both skin-mountable and implantable devices are the same, while the implantable device is passivated by PDMS layers.

A.1. Figures

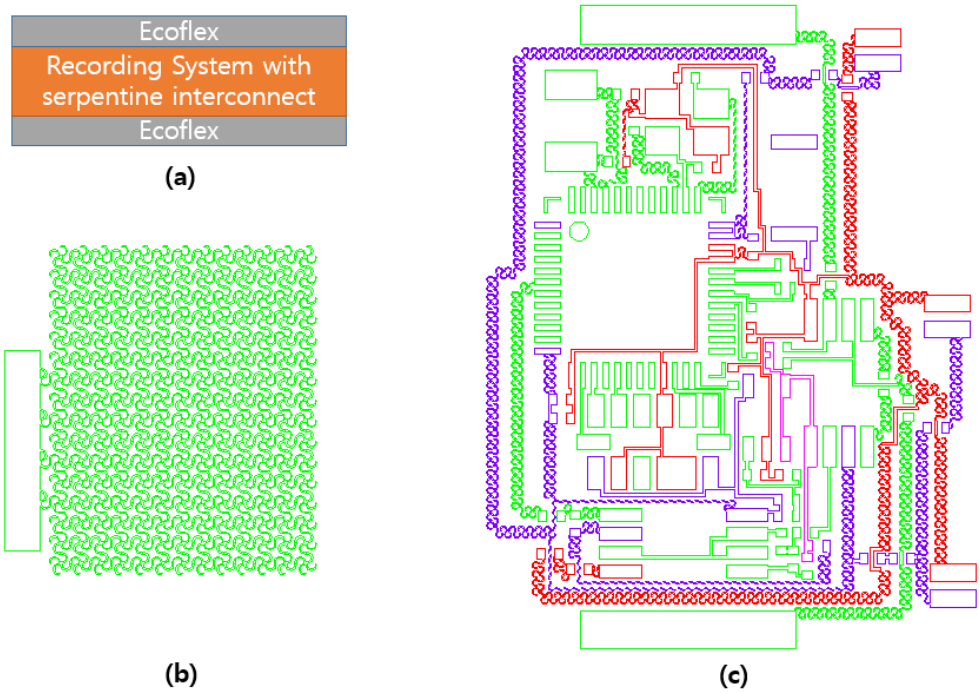

Figure A.1: (a) Simplified side view of the wireless device consisting of passivation layers of top and bottom with Ecoflex and device with serpentine interconnect for stretchability. (b) CAD layout of stretchable electrode for electrophysiological signal measurement. (c) CAD layout of overall skin-mountable device with stretchable metal interconnect.

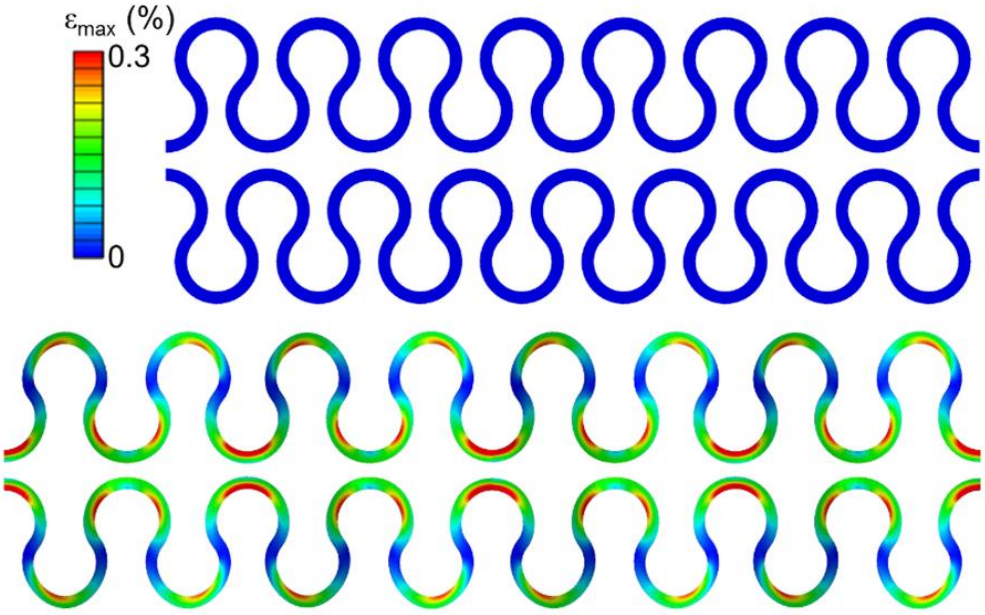

Figure A.2: The simulation result for stress profile with stretching at 20 percent.

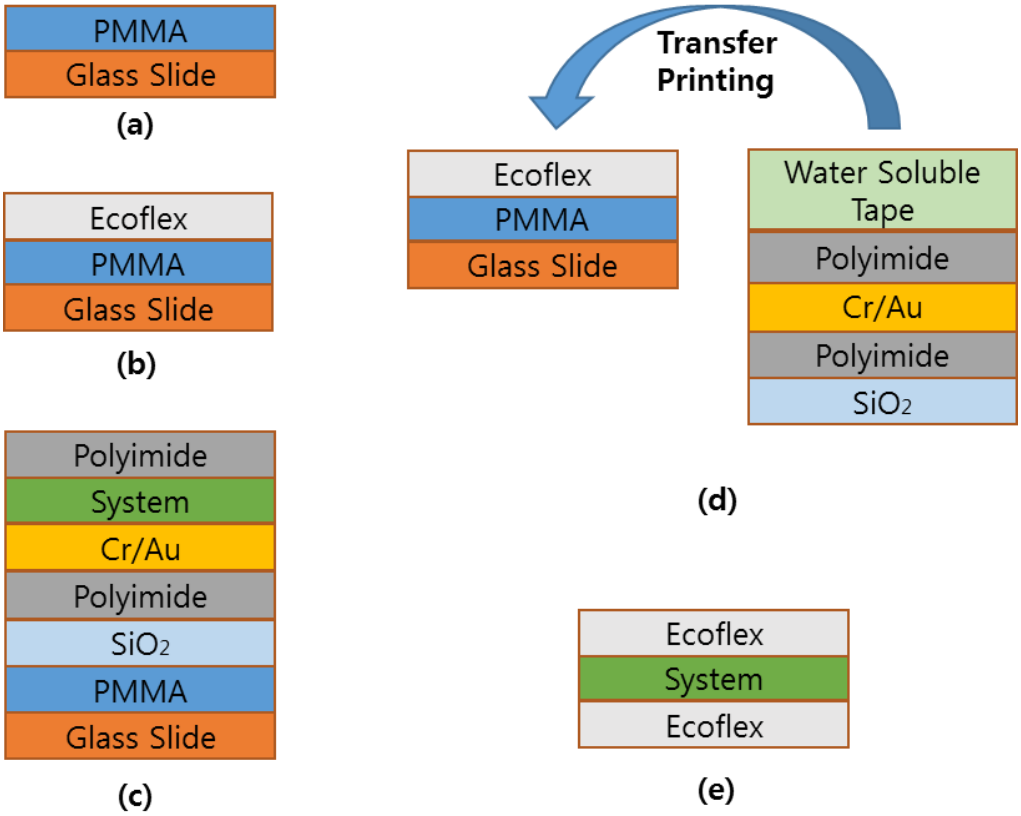

Figure A.3: Fabrication procedure steps. A simplified picture of the final device is in (e), omitting layers of polyimide, Cr/Au, and polyimide.

REFERENCES

[1] H. Berger, "Über das elektrenkephalogramm des menschen," Arch. Psychiatr Nervenkr, 87, 527-570 (1929).

[2] D.-H. Kim, N. Lu, R. Ma, Y.-S. Kim, R.-H. Kim, S. Wang, J. Wu, S.M. Won, H. Tao, A. Islam, K.J. Yu, T.-I. Kim, R. Chowdhury, M. Ying, L. Xu, M. Li, H.-J. Chung, H. Keum, M. McCormick, P. Liu, Y.-W. Zhang, F.G. Omenetto, Y. Huang, T. Coleman and J.A. Rogers, "Epidermal electronics," Science 333, 838-843 (2011).

[3] S. Xu, Y. Zhang, L. Jia, K.E. Mathewson, K.-I. Jang, J. Kim, H. Fu, X. Huang, P. Chava, R. Wang, S. Bhole, L. Wang, Y.J. Na, Y. Guan, M. Flavin, Z. Han, Y. Huang, and J.A. Rogers, "Soft microfluidic assemblies of sensors, circuits, and radios for the skin," Science 344, 70-74 (2014).

[4] T.-I. Kim, J.G. McCall, Y.H. Jung, X. Huang, E.R. Siuda, Y. Li, J. Song, Y.M. Song, H.An Pao, R.-H. Kim, C. Lu, S.D. Lee, I.-S. Song, G. Shin, R. Al-Hasani, S. Kim, M.P. Tan, Y. Huang, F.G. Omenetto, J.A. Rogers and M.R. Bruchas, "Injectable, cellular-scale optoelectronics with applications for wireless optogenetics," Science 240, 211-216 (2013).

[5] J.-W. Jeong, M.K. Kim, H. Cheng, W.-H. Yeo, X. Huang, Y. Liu, Y. Zhang, Y. Huang, and J.A. Rogers, "Capacitive epidermal electronics for electrically safe, long-term electrophysiological measurements," Advanced Healthcare Materials 3, 642-648 (2014).

[6] S.G. Deuschl, M. Lauk, and J. Timmer, "Tremor classification and tremor time series analysis,"CHAOS 5 (1), pp. 48–51 (1995).

[7] F. S. Spieker, C. Jentgens, A. Boose, and J. Dichgans, "Reliability, specificity and sensitivity of long-term tremor recordings," Electroencephalogr. Clin. Neurophysiol 97, pp. 326-331 (1995).

[8] Analog Devices. *ADXL345 datasheet.* URL: http://www.analog.com/media/en/technical-documentation/data-sheets/ADXL345.pdf

[9] Nordic Semiconductor. *nRF51822 Product Specification v3.1*. URL: https://www.nordicsemi.com/eng/Products/Bluetooth-Smart-Bluetooth-low-energy/nRF51822

[10] Texas Instruments. *CC3100MOD SimpleLink Certified Wi-Fi Network Processor Internet-of-Things Module Solution for MCU Applications.* URL: http://www.ti.com/product/CC3100MOD/datasheet

[11] Texas Instruments. *RF430FRL15xH NFC ISO 15693 Sensor Transponder.* URL: http://www.ti.com/product/rf430cl330h?keyMatch=nfc&tisearch=Search-EN-Everything

[12] CytoSpring. *PBS (Phosphate-Buffered Saline) Product Information.* URL: https://www.researchgate.net/file.PostFileLoader.html?id=52f88bfacf57d727448b45de&assetKey=AS%3A273585036300302%401442239163521.

[13] S.I. Park, D.S. Brenner, G. Shin, C.D. Morgan, B.A. Copits, H.U. Chung, M.Y. Pullen, K.N. Noh, S. Davidson, S.J. Oh, J. Yoon, K.-I. Jang, V.K. Samineni, M. Norman, J.G. Grajales-Reyes, S.K. Vogt, S.S. Sundaram, K.M. Wilson, J.S. Ha, R. Xu, T. Pan, T.-I. Kim, Y. Huang, M.C. Montana, J.P. Golden, M.R. Bruchas, R.W. Gereau and J.A. Rogers, "Soft, stretchable, fully implantable miniaturized optoelectronic systems for wireless optogenetics," Nature Biotechnology 33(12), 1280-1286 (2015).

[14] S. Mutashar, M. A. Hanna, S. A. Samad, and A. Hussain, "Analysis and optimization of spiral circular inductive coupling link for bio-implanted applications on air and within human tissue," Sensors 14(7), 11522-11541 (2014).

[15] Feig Electronic. *ANT310_310*. URL: http://www.feig.de/uploads/media/Data_sheet_ANT310_310.pdf

[16] Feig Electronic. *HF Long Range Reader ID ISC.LR(M)2500*. URL: http://www.feig.de/uploads/media/Data_sheet_ID_ISC.LR2500.pdf

[17] M.W. Baker and R. Sarpeshkar, "Feedback analysis and design of RF power links for low-power bionic systems," IEEE Trans. Biomed. Circuits Syst. 1 (1), pp. 28-38 (2007)

[18] M. Kiani, U-M. Jow, and M. Ghovanloo, "Design and optimization of a 3-coil inductive link for efficient wireless power transmission," IEEE Trans. Biomed. Circuits Syst, 5 (6), pp. 579-591 (2011)

[19] A. Kurs, A. Karalis, R. Moffatt, J.D. Joannopoulos, P. Fisher, and M. Soljacic. "Wireless power transfer via strongly coupled magnetic resonances," Science 317, 83–86 (2007).

[20] B.L. Cannon, J.F. Hoburg, D.D. Stancil, and S.C. Goldstein, "Magnetic resonant coupling as a potential means for wireless power transfer to multiple small receivers," IEEE Trans. Power Electron 24, 1819–1825 (2009).

[21] Y. Su, Z. Liu, S. Kim, J. Wu, Y. Huang, and J.A. Rogers, "Mechanics of stretchable electronics with high fill factors," International Journal of Solids and Structures 49, 3416-3421 (2012).

[22] S. Wang, M. Li, J. Wu, D.-H. Kim, N. Lu, Y. Su, Z. Khang, Y. Huang, and J.A. Rogers, "Mechanics of epidermal electronics," Journal of Applied Mechanics 79, 031022-1 (2012).